Electronic structure, hyperfine interactions, and magnetic properties for iron octahedral sulfides

M. Braga
Departamento de Química Fundamental, Universidade Federal de Pernambuco, 50 739 Recife, Pernambuco, Brazil

S. K. Lie
Instituto de Física, Universidade Federal Fluminense, Caixa Postal 296, 24 210 Niterói, Rio de Janeiro, Brazil

C. A. Taft
Centro Brasileiro de Pesquisas Físicas, rua Dr. Xavier Sigaud 150, Urca, 22 290 Rio de Janeiro, Rio de Janeiro, Brazil

W. A. Lester, Jr.
Department of Chemistry, University of California, Berkeley, California 94720
and Materials and Chemical Sciences Division, Lawrence Berkeley Laboratory, University of California, Berkeley, California 94720
(Received 30 June 1988)

Spin-polarized multiple-scattering calculations have been performed for FeS_6^{n-} ($n=8,9,10$) clusters in order to study the electronic structure of the iron atom octahedrally coordinated to sulfur. The calculated total spin and charge densities in connection with the $3d$ and $4s$ atomic population are used to interpret the Mössbauer hyperfine parameters. A detailed discussion of the hyperfine interaction and magnetic properties is given for the spinel greigite (Fe_3S_4). Possible existence of an Fe(IV) state is discussed.

I. INTRODUCTION

The metallic sulfides have been known and valued as sources of metals from the earliest times and are the most important group of ore minerals, constituting the raw materials, for most of the world supply of nonferrous metals. The technologically important electrical and magnetic properties of these systems have stimulated, in general, numerous detailed measurements and the development of electronic structure models.[1-37]

Iron is by far the most abundant transition element in the earth's crust and occurs frequently in different oxidation states with the chalcogenide and pnictide elements of which sulfur is the most important. Fe(II) and Fe(III) sulfur octahedral units of the type investigated in this paper are the basic polyhedral units in a large number of important minerals among whose electrical properties one finds semiconductivity (pyrite), metallic conductivity (FeS), and ferroelectricity (troillite), and among whose magnetic properties one finds ferromagnetism, antiferromagnetism, and ferrimagnetism. A better understanding of the electronic structure and chemical bonding in these units is necessary to elucidate the wide diversity of optical, electrical, and magnetic properties, as well as hyperfine interactions and other important solid-state effects observed in octahedral iron sulfides.

We may classify these sulfides into two groups, the first distinguished by simple quadrupolar splittings such as pyrite and marcassite (FeS_2), and the second group characterized by magnetic hyperfine splitting such as phyrothite ($Fe_{1-x}S$), mackinavite (FeS_{1-x}), greigite (Fe_3S_4), and smythite (Fe_3S_4)

Regarding the first group, we note that x-ray, Mössbauer, and magnetic-susceptibility measurements indicate iron in both pyrite and marcassite to be in the low-spin Fe^{2+} configuration. Since there are no unpaired electrons in the Fe atoms, the occurrence of an electric field gradient in pyrite has been the subject of various interpretations. There are also conflicting views on the chemical bonding in pyrite. Burns and Vaughan[28] have suggested that the paired electrons in the nonbonding t_{2g} orbitals may form π bonds with vacant $3d$ t_{2g} orbitals of the sulfur atoms, resulting in the backdonation from Fe $3d$ electrons. However, Kjekshus and Nicholson[29] critically evaluated Mössbauer and bond-length data and found no evidence to support π backdonation between metal and nonmetal atoms. Regarding the second group, we note that smythite has a hexagonal layer structure akin to that of phyrrotite. Of significant research interest is greigite,[31] a rare inverse spinel mineral isomorphic with the oxide magnetite, which has been found naturally as a black magnetic powder in tertiary lacustric sediments, vegetal ooze, and a mammoth's tusk and is probably formed by bacteriological reduction of iron in sedimentary deposits showing no tendency to decompose in air at room temperature.

The Mössbauer spectroscopic studies of greigite by Coey *et al.*[32] have indicated hyperfine fields of ~ 311 kOe at both A and B sites, suggesting fast electronic relaxation between Fe^{2+} and Fe^{3+} B sites. The magnetic moment predicted for the Néel configuration is equal to or greater than $4\mu_B$, which is too large to account for the measured magnetic moment of $(2.2\pm0.3)\mu_B$.

In contrast to the iron oxides, a large number of phases are found in the compounds of iron with sulfur. Consequently, the Mössbauer spectra of low- and high-spin

Fe^{2+} as well as high-spin Fe^{3+} in octahedral coordination has been extensively investigated due to the large variety of systems available and to the relevance of these compounds to a better comprehension of the Fe—S covalent bonds as well as the important occurrence of these clusters in biological systems. In addition, synthesis and Mössbauer-effect studies of the very unusual formal oxidation state Fe(IV) and several intermediate-spin Fe(III) complexes have also been reported.[35,36]

Regarding previous theoretical work of octahedral iron sulfides, we note that Li *et al.*[34] have investigated the electronic structure and spectrum of pyrite using the self-consistent-field $X\alpha$ (SCF-$X\alpha$) scattered-wave method. Tossel[26] also used this method to study the electronic structure of ferrous iron in octahedral coordination with sulfur. Lauer *et al.*[27] carried out electronic-structure calculations based on a self-consistent-charge, linear combination of atomic orbitals (LCAO) band-structure method for pyrite.

Previously we investigated the electronic structure, hyperfine interactions, and radial densities in the Fe^{1+}, Fe^{2+}, Fe^{3+}, and Fe^{4+} tetrahedral iron sulfides using the multiple-scattering $X\alpha$ (MS $X\alpha$) model.[21–24] In order to elucidate the many conflicting interpretations of the experimental data on octahedral iron sulfides, in the present paper we have investigated the Fe^{2+}, Fe^{3+}, and Fe^{4+} octahedral iron sulfides in both high- and low-spin configurations. Calculations have also been made with partial waves $l=1$ and 2 in the S sphere in order to clarify conflicting discussions on possible π-backdonation effects in pyrite. Particular interest has been placed on interpreting the conflicting Mössbauer and magnetic-susceptibility experimental data in the spinel greigite.

II. COMPUTATIONAL DETAILS

The MS $X\alpha$ method,[38] in the muffin-tin form and using Slater $X\alpha$ local exchange, has been applied to the FeS_6^{10-}, FeS_6^{9-}, and FeS_6^{8-} clusters in both the high- and low-spin configurations. For low-spin Fe^{2+} the Fe-S distance of 2.26 Å, corresponding to pyrite has been used. For the other configurations the Fe-S distance of 2.46 Å found in greigite (Fe_3S_4) has been retained.[30] The values of the exchange parameter α used in these calculations were taken from Schwarz.[39] For the Fe atom, Pauling's[40] Fe covalent octahedral radius of 1.23 Å was assumed. A Watson sphere with appropriate charge was introduced to stabilize the various clusters. All the electrons (core plus valence) have been included in each SCF cycle and calculations were carried out to self-consistency. In the Fe and outer regions we have used $l=0$ for orbitals of a_{1g} symmetry, $l=1$ for t_{1u}, $l=2$ for e_g and t_{2g}, and $l=3$ for t_{1g}. In the S spheres we have retained contributions up to $l=2$. Larsson's technique,[41] discussed in our previous papers,[21–24,42] has been used to derive atomic populations.

III. ORBITALS, ORBITAL ENERGIES, AND ELECTRON POPULATION

The orbital energies, orbital characters, and the charge distributions within the different muffin-tin regions for the FeS_6^{10-} (singlet and quintuplet), FeS_6^{9-} (sextuplet and doublet), and FeS_6^{8-} (quintuplet and triplet) clusters corresponding, respectively, to high- and low-spin Fe^{2+}, Fe^{3+}, and Fe^{4+} in sulfur octahedral coordination are given in Tables I–IV and labeled according to the irreducible representations of the symmetry group O_h. The calculated energy levels for these clusters in the ground state are given in Figs. 1–3. For all the clusters, the a_{1g}, t_{1u}, and $4e_g$ orbitals correspond to sulfur 3*s* levels. For the high-spin FeS^{10-} cluster, the spin-up $5e_g$ and both the spin-up and spin-down $3t_{2g}$ orbitals correspond to the iron crystal-field 3*d* levels. For the low-spin FeS_6^{10-} the $3t_{2g}$ level is the Fe 3*d* level. In the case of the high-spin FeS_6^{9-} and for both high- and low-spin configurations of FeS_6^{8-}, the spin-up $5e_g$ and $2t_{2g}$ levels are Fe 3*d* levels. For low-spin FeS_6^{8-}, the spin-down $3t_{2g}$ (occupied by one electron) correlates with the Fe 3*d* level. It is then possible to see that when passing from FeS_6^{9-} to FeS_6^{8-} one does not get an Fe^{4+} cluster; instead one has different possibilities depending on the spin configuration of the initial FeS_6^{9-} (see below). Finally, the low-spin FeS_6^{9-} has the Fe 3*d* charge distributed between both the spin-up and spin-down $3t_{2g}$ levels; the e_g level is empty. Different percentages of Fe 3*d* – S 3*p* admixture are found for all these levels, the largest occurring in the FeS_6^{10-} cluster. This can explain the comparatively large 3*d* splitting found for this cluster.

The remaining e_g and t_{2g} levels arise from the S 3*p* orbitals and some mixing with the Fe 3*d* component is also found (see Tables I–IV). For the $8a_{1g}$ level we find a significant 4*s* component (in all cases, this component is $\sim 30\%$). The $8t_{1u}$, $9t_{1u}$, $2t_{1g}$, and $2t_{2u}$ are largely nonbonding orbitals. It is interesting to note the small magnitude of the 4*p* component found for the t_{1u} levels. This feature is consistent with what we previously found for tetrahedral iron-sulfide clusters and indicates that the Fe 4*p* orbital does not significantly contribute to Fe—S bonding in both tetrahedral and octahedral sulfides. However, the Fe 4*s* participation is large and consistent with our previous results for tetrahedral systems. The valence-band width of FeS_6^{10-} is 11.75 eV for the singlet and 13.54 eV for the quintuplet. For the FeS_6^{9-} cluster it is 11.78 eV for the sextuplet and 11.96 eV for the doublet, whereas for FeS_6^{8-} it is 11.84 eV for the quintuplet and 12.56 eV for the triplet configurations.

According to Burns and Vaughan,[28] the paired electrons in nonbonding t_{2g} orbitals are capable of forming π bonds with vacant t_{2g}-type 3*d* orbitals of the sulfur atoms. This should result in increased energy separation between nonbonding t_{2g} and antibonding e_g^* levels. Since low-spin Fe(II) contains no electrons in e_g^* orbitals to repel sulfur ligands, π bonding should be most efficient in FeS_2. The energy separation (Δ) between nonbonding t_{2g} and antibonding e_g^* orbitals is computed to be -1.97 eV in pyrite. The low-spin configuration of pyrite is an indication of the strength of the ligand field.

Extensive covalent bonding between transition-metal and sulfur atoms leads to the delocalization of electrons in antibonding e_g^* and t_{2g}^* orbitals. Electrons excited into e_g^* orbitals should become delocalized from the cation

and be analogous to effectively free electrons of metals. The lowest unoccupied orbital in the FeS_6^{10-} (singlet) cluster is effectively conductionlike with 70% of its charge in the extramolecular region. The highest occupied t_{2g} Fe $3d$-like level has 77% of its electronic charge in the Fe atomic region and only 3% contained within the six S atomic regions and therefore is localized and largely nonbonding.

In pyrite the main bonding molecular orbitals form the filled σ band and the corresponding antibonding orbitals the empty σ^* band constituting the main valence and conduction bands, respectively. The Fe $3d$ orbitals lie between these bands. The t_{2g} orbitals are essentially localized on the cation, but the e_g^* orbitals form a band through overlap with sulfur. Thus conduction in pyrite occurs when electrons are excited into the band formed from e_g^* orbitals. In these sulfides, the valence-band energy levels are composed of sulfur $3s$- and $3p$-type orbitals. The conduction orbitals of the metal, s and p with added d orbitals, whose relative energies may vary widely, can overlap with the sulfur atoms to form bands. In the ferromagnetic, metallic spinels of the transition-metal chalcogenides, the outer d electrons may be either localized and spontaneously magnetic, collective without spontaneous magnetism or transitional between these two extremes. Covalent mixing between anionic s and p orbitals and cationic s as well as d orbitals sensitively influence the magnetic and electrical properties.

The possibility of a Fe $3d(t_{2g})\rightarrow$S $3d$ backdonation in pyrite has been suggested and discussed by Burns and Vaughan.[28] Kjekshus and Nicholson[29] evaluated Mössbauer and bond-length data for pyrite and other compounds and found no evidence to support π backdonation in these compounds. In Tables V–VIII we give the electron populations on Fe for molecular orbitals of a_{1g}, e_g, and t_{2g} symmetries for the FeS_6^{10-} (singlet and quintuplet), FeS_6^{9-} (sextuplet and doublet), and FeS_6^{8-} (quintuplet and triplet) clusters. We note in Tables V and VI that the net atomic charge on Fe for $l=1$ and 2 on the S sphere does not change significantly, suggesting the absence of significant π backdonation in these systems. The first unoccupied t_{2g} orbital of ligand character is largely a S $3p$ orbital with little or no $3d$ admixture. For all cases, a strong covalency for the Fe—S bond is found, which

TABLE I. Orbital energies and orbital characters for low-spin FeS_6^{10-} cluster ($d_{Fe\text{-}S}=2.26$ Å).

Orbital	Orbital energy ($-$Ry)	Charge[a] in muffin-tin sphere Fe	S[b]	Inter-atomic	Outer sphere	Orbital character
		FeS_6^{10-} (l up to 2 on S)				
$7a_{1g}$	1.125	3.79	10.38	31.25	2.66	S $3s$
$7t_{1u}$	1.056	1.47	11.38	26.83	3.39	S $3s$
$4e_g$	1.030	2.16	11.84	22.58	4.18	S $3s$
$8a_{1g}$	0.471	11.92	6.96	37.99	8.33	S $3p$, Fe $4s$
$2t_{2g}$	0.459	8.38	5.71	47.88	9.48	S $3p$, Fe $3d$
$8t_{1u}$	0.430	2.76	6.66	53.84	3.43	S $3p$
$5e_g$	0.369	34.58	6.07	19.64	9.36	S $3p$, Fe $3d$
$2t_{2u}$	0.317	0.21	7.73	41.56	11.86	S $3p$
$9t_{1u}$	0.286	3.31	7.28	28.83	24.15	S $3p$
$2t_{1g}$	0.261	0.00	9.12	45.24	0.00	S $3p$
$3t_{2g}$[c]	0.160	76.56	0.50	10.16	10.30	Fe $3d$, S $3p$
		FeS_6^{10-} (l up to 1 on S)				
$7a_{1g}$	1.124	3.75	10.36	31.41	2.66	S $3s$
$7t_{1u}$	1.055	1.46	11.37	26.91	3.41	S $3s$
$4e_g$	1.029	2.12	11.84	22.66	4.18	S $3s$
$8a_{1g}$	0.470	11.42	6.95	38.72	8.16	S $3p$, Fe $4s$
$2t_{2g}$	0.458	7.49	5.74	48.22	9.84	S $3p$, Fe $3d$
$8t_{1u}$	0.437	2.72	6.65	53.90	3.47	S $3p$
$5e_g$	0.363	32.52	6.23	20.22	9.85	S $3p$, Fe $3d$
$2t_{2u}$	0.316	0.21	7.75	41.68	11.61	S $3p$
$9t_{1u}$	0.283	3.27	7.37	28.58	23.93	S $3p$
$2t_{1g}$	0.259	0.00	9.22	44.70	0.00	S $3p$
$3t_{2g}$[c]	0.141	79.41	0.24	9.16	10.00	Fe $3d$, S $3p$

[a]Units of percent of one electron charge.
[b]Units of percent of charge in each S sphere.
[c]Highest occupied level.

TABLE II. Orbital energies and orbital characters for high-spin FeS_6^{10-} cluster ($d_{Fe\text{-}S}=2.46$ Å).

Orbital	Orbital energy (−Ry)	Charge[a] in muffin-tin sphere: Fe	S[b]	Inter-atomic	Outer sphere	Orbital character
			FeS_6^{10-} (l up to 2 on S)			
$7a_{1g}^{\uparrow}$	1.056	2.19	12.69	20.29	1.41	S 3s
$7a_{1g}^{\downarrow}$	1.049	1.87	12.75	20.21	1.44	S 3s
$7t_{1u}^{\uparrow}$	1.015	0.76	13.50	16.54	1.72	S 3s
$7t_{1u}^{\downarrow}$	1.010	0.69	13.51	16.51	1.74	S 3s
$4e_g^{\uparrow}$	1.002	1.52	13.74	13.88	2.15	S 3s
$4e_g^{\downarrow}$	0.995	0.93	13.82	13.92	2.20	S 3s
$8a_{1g}^{\uparrow}$	0.423	11.77	8.64	30.82	5.57	S 3p, Fe 4s
$8a_{1g}^{\downarrow}$	0.404	9.73	8.86	31.18	5.91	S 3p, Fe 4s
$5e_g^{\uparrow}$	0.420	65.66	3.75	8.92	2.93	Fe 3d, S 3p
$5e_g^{\downarrow}$	0.301	19.83	8.84	17.81	9.34	S 3p, Fe 3d
$2t_{2g}^{\uparrow}$	0.420	45.81	4.33	25.39	2.84	S 3p, Fe 3d
$2t_{2g}^{\downarrow}$	0.373	3.69	7.73	42.61	7.32	S 3p, Fe 3d
$8t_{1u}^{\uparrow}$	0.368	2.43	8.72	42.69	2.58	S 3p
$8t_{1u}^{\downarrow}$	0.361	2.02	8.67	43.36	2.60	S 3p
$3t_{2g}^{\uparrow}$	0.305	50.63	4.01	19.27	6.02	S 3p, Fe 3d
$2t_{2u}^{\uparrow}$	0.286	0.10	10.09	31.98	7.41	S 3p
$2t_{2u}^{\downarrow}$	0.283	0.10	10.06	32.06	7.47	S 3p
$9t_{1u}^{\uparrow}$	0.268	1.80	9.48	24.77	16.56	S 3p
$9t_{1u}^{\downarrow}$	0.262	1.67	9.50	24.36	16.95	S 3p
$2t_{1g}^{\uparrow}$	0.243	0.00	10.62	36.27	0.00	S 3p
$2t_{1g}^{\downarrow}$	0.240	0.00	10.60	36.38	0.00	S 3p
$6e_g^{\uparrow}$	0.159	32.43	6.95	11.38	14.48	S 3p, Fe 3d
$3t_{2g}^{\downarrow}$[c]	0.061	72.70	0.28	9.81	15.81	Fe 3d, S 3p
			FeS_6^{10-} (l up to 1 on S)			
$7a_{1g}^{\uparrow}$	1.059	2.19	12.68	20.34	1.41	S 3s
$7a_{1g}^{\downarrow}$	1.053	1.86	12.74	20.25	1.44	S 3s
$7t_{1u}^{\uparrow}$	1.018	0.76	13.50	16.53	1.72	S 3s
$7t_{1u}^{\downarrow}$	1.013	0.69	13.50	16.54	1.74	S 3s
$4e_g^{\uparrow}$	1.004	1.52	13.74	13.90	2.15	S 3s
$4e_g^{\downarrow}$	0.998	0.92	13.82	13.94	2.20	S 3s
$8a_{1g}^{\uparrow}$	0.426	11.50	8.63	31.13	5.57	S 3p, Fe 4s
$8a_{1g}^{\downarrow}$	0.407	9.48	8.86	31.46	5.92	S 3p, Fe 4s
$5e_g^{\uparrow}$	0.422	65.34	3.74	9.16	3.08	Fe 3d, S 3p
$5e_g^{\downarrow}$	0.303	18.90	8.92	18.00	9.60	S 3p, Fe 3d
$2t_{2g}^{\uparrow}$	0.422	45.98	4.29	25.33	2.96	S 3p, Fe 3d
$2t_{2g}^{\downarrow}$	0.373	3.59	8.14	40.21	7.36	S 3p, Fe 3d
$8t_{1u}^{\uparrow}$	0.371	2.39	8.69	42.90	2.59	S 3p, Fe 3d
$8t_{1u}^{\downarrow}$	0.365	1.99	8.65	43.52	2.61	S 3p
$3t_{2g}^{\uparrow}$	0.308	51.16	3.97	19.21	5.83	Fe 3d, S 3p
$2t_{2u}^{\uparrow}$	0.288	0.10	10.10	31.99	7.29	S 3p
$2t_{2u}^{\downarrow}$	0.285	0.10	10.08	32.04	7.37	S 3p
$9t_{1u}^{\uparrow}$	0.270	1.78	9.51	24.69	16.47	S 3p
$9t_{1u}^{\downarrow}$	0.265	1.65	9.53	24.24	16.93	S 3p
$2t_{1g}^{\uparrow}$	0.245	0.00	10.66	36.06	0.00	S 3p
$2t_{1g}^{\downarrow}$	0.242	0.00	10.64	36.15	0.00	S 3p

TABLE II. (*Continued*).

Orbital	Orbital energy (−Ry)	Charge[a] in muffin-tin sphere Fe	S[b]	Inter-atomic	Outer sphere	Orbital character
$6e_g^{\uparrow}$	0.158	33.82	6.79	10.95	14.46	S 3*p*, Fe 3*d*
$3t_{2g}^{\downarrow}$[c]	0.052	71.22	0.02	9.32	19.34	Fe 3*d*, S 3*p*

[a]In units of percent of one electron charge.
[b]In units of percent of charge in each S sphere.
[c]Highest occupied level.

leads to a partial population of the Fe 3*d* spin-down levels. Some charge delocalization is also found. Note that the low-spin configurations are more covalent and thus have lower effective charges than the high-spin configurations.

The Fe^{3+} low-spin configuration and the Fe^{4+} high- and low-spin configurations are rarely found. For the Fe^{3+} low-spin configuration, we obtain a net charge on Fe which is very close to that of the high-spin cluster. However, the charge distribution between the spin-up and -down 3*d* orbitals for both complexes is quite different. For the Fe^{4+} high-spin (quintuplet) cluster we get a total charge on Fe, indicating a configuration which clearly resembles the Fe^{3+} high-spin (sextuplet) configuration. A similar correspondence is found between the Fe^{4+} low-spin (triplet) configuration and the Fe^{2+} high-spin (quintuplet) configuration.

It is interesting to compare the effect of removing one electron from the tetrahedral FeS_4^{5-} and the octahedral FeS_6^{9-} clusters. For the tetrahedral cluster FeS_4^{5-} the highest occupied molecular orbital (HOMO) is the $10t_2$, which is a ligand level, and the removal of one electron from this level will not significantly change the electronic configuration of the Fe atom. For the FeS_6^{9-} high-spin cluster the situation is similar. The HOMO is the $6e_g$ orbital, which is also a ligand level. By removal of one electron from this orbital we obtain a high-spin FeS_6^{8-} cluster, where the electronic configuration and total charge is close to that of the FeS_6^{9-} high-spin cluster (see Tables VII and VIII). In the low-spin case, the HOMO for the FeS_6^{9-} cluster is $3d\ t_{2g}^{\downarrow}$. The removal of one electron from this level could have given a FeS_6^{8-} cluster; however, the result was different. Charge transfer from the ligands to the metal was found and the final configuration of the Fe atom was not the expected Fe^{4+}, but close to the configuration of the low-spin FeS_6^{10-} cluster. Charge transfer from the ligands to the metal implies that the sulfur is oxidized and the Fe is reduced ($Fe^{4+} \rightarrow Fe^{2+}$). From the present results we can conclude that the presence of Fe(IV) minerals containing only Fe-S is unlikely. Only some di-thio ligands were found to stabilize these high-valence states in spite of the easily oxidizable sulfur atoms.[36]

IV. HYPERFINE INTERACTIONS, MAGNETIC MOMENTS, AND RADIAL DENSITIES

The octahedral iron-sulfide minerals such as pyrite and greigite contain Fe with different degrees of covalency, spin, and charge configuration and should thus provide an interesting group of systems for both experimental and theoretical research.

Pyrite has an Fe-S distance of 2.26 Å and covalent ferrous Fe is in the low-spin ^1S configuration and thus has no magnetic hyperfine interaction. Greigite indicates magnetic hyperfine interactions at both tetrahedral *A* and octahedral *B* sites. Our calculated FeS_6^{9-} (sextuplet) and FeS_6^{10-} (quintuplet) clusters are representative of the inequivalent iron sites in greigite with the inverse spinel structure having Fe^{3+} at *A* tetrahedral sites and Fe^{2+} and Fe^{3+} at *B* octahedral sites.

The Mössbauer-spectroscopic studies of greigite are, however, conflicting. Vaughan and Ridout[33] studied greigite and concluded that ferrous and ferric ions were magnetically ordered at both tetrahedral and octahedral sites. Coey *et al.*[32] studied the spectra at low temperatures and in external magnetic fields and concluded that greigite is the sulfur analog of magnetite. Further, they observed only a single species in the octahedral sites and suggested electron hopping as in the oxide magnetite.

It was thus considered of interest to investigate the magnetic hyperfine fields, via the Fermi-contact term, at the high-spin Fe^{2+} and Fe^{3+} nucleus in the FeS_6^{9-} (sextuplet) and FeS_6^{10-} (quintuplet) clusters. The hyperfine fields at the Fe^{3+} and Fe^{4+} nucleus in the FeS_6^{9-} (doublet) and FeS_6^{8-} (quintuplet and triplet) clusters were also investigated.

The magnetic hyperfine field at the Fe nucleus, measured by Mössbauer spectroscopy, may be expressed as

$$H_{\text{eff}} = H_c + H_{\text{orb}} + H_{\text{dip}} \ . \tag{1}$$

The first term H_c is the Fermi-contact term, which is given by

$$H_c = \tfrac{8}{3}\pi g \mu_B S \, | \, \psi(0) \, | \, ^2_{\uparrow} - | \, \psi(0) \, | \, ^2_{\downarrow} \ , \tag{2}$$

where g is the electronic spectroscopic splitting factor,

TABLE III. Orbital energies and orbital characters for FeS_6^{9-} clusters.

Orbital	Orbital energy (−Ry)	Charge[a] in muffin-tin sphere: Fe	S[b]	Inter-atomic	Outer sphere	Orbital character
		High-spin FeS_6^{9-} cluster				
$7a_{1g}^{\uparrow}$	1.062	2.44	12.66	20.29	1.33	S 3*s*
$7a_{1g}^{\downarrow}$	1.049	2.07	12.72	20.27	1.36	S 3*s*
$7t_{1u}^{\uparrow}$	1.020	0.81	13.51	16.51	1.65	S 3*s*
$7t_{1u}^{\downarrow}$	1.009	0.74	13.53	16.45	1.66	S 3*s*
$4e_g^{\uparrow}$	1.008	2.35	13.64	13.76	2.02	S 3*s*
$4e_g^{\downarrow}$	0.994	1.15	13.82	13.86	2.09	S 3*s*
$8a_{1g}^{\uparrow}$	0.437	13.12	8.52	30.84	4.94	S 3*p*, Fe 4*s*
$8a_{1g}^{\downarrow}$	0.410	10.76	8.80	31.31	5.16	S 3*p*, Fe 4*s*
$5e_g^{\uparrow}$	0.546	82.67	1.79	5.38	1.18	Fe 3*d*, S 3*p*
$5e_g^{\downarrow}$	0.331	36.10	7.11	14.95	6.32	S 3*p*, Fe 3*d*
$2t_{2g}^{\uparrow}$	0.540	87.43	0.69	8.18	0.24	Fe 3*d*, S 3*p*
$2t_{2g}^{\downarrow}$	0.375	9.28	7.74	38.36	5.95	S 3*p*, Fe 3*d*
$8t_{1u}^{\uparrow}$	0.372	2.76	8.82	41.91	2.44	S 3*p*
$8t_{1u}^{\downarrow}$	0.359	2.27	8.76	42.80	2.40	S 3*p*
$3t_{2g}^{\uparrow}$	0.348	9.51	7.89	35.53	7.66	S 3*p*, Fe 3*d*
$2t_{2u}^{\uparrow}$	0.287	0.11	10.25	31.69	6.71	S 3*p*
$2t_{2u}^{\downarrow}$	0.277	0.10	10.24	31.81	6.66	S 3*p*
$9t_{1u}^{\uparrow}$	0.269	1.87	9.73	24.99	14.77	S 3*p*
$9t_{1u}^{\downarrow}$	0.256	1.75	9.81	24.64	14.77	S 3*p*
$2t_{1g}^{\uparrow}$	0.246	0.00	10.71	35.72	0.00	S 3*p*
$2t_{1g}^{\downarrow}$	0.236	0.00	10.68	35.90	0.00	S 3*p*
$6e_g^{\uparrow}$[c]	0.196	15.62	9.19	15.83	13.42	S 3*p*, Fe 3*d*
$3t_{2g}^{\downarrow}$	0.168	83.93	0.75	8.33	3.22	Fe 3*d*, S 3*p*
		Low-spin FeS_6^{9-} cluster				
$7a_{1g}^{\uparrow}$	1.046	2.03	12.75	20.10	1.37	S 3*s*
$7a_{1g}^{\downarrow}$	1.052	1.88	12.82	19.86	1.36	S 3*s*
$7t_{1u}^{\uparrow}$	1.006	0.72	13.53	16.41	1.66	S 3*s*
$7t_{1u}^{\downarrow}$	1.013	0.69	13.57	16.21	1.65	S 3*s*
$4e_g^{\uparrow}$	0.992	1.23	13.82	13.77	2.09	S 3*s*
$4e_g^{\downarrow}$	0.999	1.01	13.87	13.70	2.08	S 3*s*
$8a_{1g}^{\uparrow}$	0.405	10.67	8.82	31.06	5.37	S 3*p*, Fe 4*s*
$8a_{1g}^{\downarrow}$	0.403	9.81	8.96	31.00	5.40	S 3*p*, Fe 4*s*
$2t_{2g}^{\uparrow}$	0.377	16.04	7.11	35.90	5.41	S 3*p*, Fe 3*d*
$2t_{2g}^{\downarrow}$	0.371	5.80	8.14	38.89	6.44	S 3*p*, Fe 3*d*
$8t_{1u}^{\uparrow}$	0.354	2.26	8.82	42.32	2.49	S 3*p*
$8t_{1u}^{\downarrow}$	0.358	2.10	8.91	41.98	2.47	S 3*p*
$5e_g^{\uparrow}$	0.351	47.10	5.86	12.65	5.10	S 3*p*, Fe 3*d*
$5e_g^{\downarrow}$	0.314	27.32	8.13	16.25	7.67	S 3*p*, Fe 3*d*
$2t_{2u}^{\uparrow}$	0.274	0.10	10.24	31.61	6.85	S 3*p*
$2t_{2u}^{\downarrow}$	0.279	0.10	10.30	31.41	6.69	S 3*p*
$9t_{1u}^{\uparrow}$	0.254	1.71	9.74	24.40	15.45	S 3*p*
$9t_{1u}^{\downarrow}$	0.258	1.64	9.85	24.16	15.10	S 3*p*
$2t_{1g}^{\uparrow}$	0.232	0.00	10.73	35.62	0.00	S 3*p*
$2t_{1g}^{\downarrow}$	0.237	0.00	10.78	35.33	0.00	S 3*p*
$3t_{2g}^{\uparrow}$	0.220	79.02	1.36	9.44	3.37	Fe 3*d*, S 3*p*
$3t_{2g}^{\downarrow}$[c]	0.167	85.64	0.40	7.84	4.10	Fe 3*d*, S 3*p*
$6e_g^{\uparrow}$	0.096	51.12	4.61	7.05	14.15	Fe 3*d*, S 3*p*

[a]In units of percent of one electron charge.
[b]In units of percent of charge in each S sphere.
[c]Highest occupied level.

TABLE IV. Orbital energies and orbital characters for FeS_6^{8-} clusters.

Orbital	Orbital energy (−Ry)	Charge[a] in muffin-tin sphere: Fe	S[b]	Inter-atomic	Outer sphere	Orbital character
		High-spin FeS_4^{8-} cluster				
$7a_{1g}^{\uparrow}$	1.074	2.45	12.71	20.05	1.25	S 3*s*
$7a_{1g}^{\downarrow}$	1.069	2.08	12.80	19.87	1.27	S 3*s*
$7t_{1u}^{\uparrow}$	1.033	0.81	13.57	16.24	1.56	S 3*s*
$7t_{1u}^{\downarrow}$	1.029	0.74	13.59	16.17	1.56	S 3*s*
$4e_g^{\uparrow}$	1.021	2.38	13.68	13.62	1.91	S 3*p*
$4e_g^{\downarrow}$	1.015	1.19	13.86	13.66	1.97	S 3*p*
$8a_{1g}^{\uparrow}$	0.446	13.34	8.59	30.69	4.41	S 3*p*, Fe 4*s*
$8a_{1g}^{\downarrow}$	0.426	11.02	8.90	30.98	4.60	S 3*p*, Fe 4*s*
$5e_g^{\uparrow}$	0.559	82.96	1.78	5.30	1.07	S 3*p*, Fe 4*s*
$5e_g^{\downarrow}$	0.357	40.76	6.68	13.91	5.23	Fe 3*d*, S 3*p*
$2t_{2g}^{\uparrow}$	0.554	87.97	0.66	7.90	0.20	Fe 3*d*, S 3*p*
$2t_{2g}^{\downarrow}$	0.391	12.05	7.67	36.88	5.05	S 3*p*, Fe 3*d*
$8t_{1u}^{\uparrow}$	0.380	2.83	8.98	41.05	2.25	S 3*p*
$8t_{1u}^{\downarrow}$	0.374	2.37	9.01	41.35	2.23	S 3*p*
$3t_{2g}^{\uparrow}$	0.355	9.01	8.14	35.32	6.82	S 3*p*, Fe 3*d*
$2t_{2u}^{\uparrow}$	0.295	0.11	10.44	31.27	5.95	S 3*p*
$2t_{2u}^{\downarrow}$	0.292	0.10	10.46	31.21	5.91	S 3*p*
$9t_{1u}^{\uparrow}$	0.275	1.88	10.08	24.96	12.70	S 3*p*
$9t_{1u}^{\downarrow}$	0.270	1.74	10.17	24.53	12.68	S 3*p*
$2t_{1g}^{\uparrow}$	0.256	0.00	10.80	35.19	0.00	S 3*p*
$2t_{1g}^{\downarrow}$	0.253	0.00	10.82	35.11	0.00	S 3*p*
$6e_g^{\uparrow}$[c]	0.204	15.41	9.45	16.25	11.66	S 3*p*, Fe 3*d*
$3t_{2g}^{\downarrow}$	0.207	82.28	1.08	8.62	2.64	Fe 3*d*, S 3*p*
		Low-spin FeS_4^{8-} cluster				
$7a_{1g}^{\uparrow}$	1.067	2.29	12.75	19.95	1.27	S 3*s*
$7a_{1g}^{\downarrow}$	1.068	1.97	12.83	19.77	1.28	S 3*s*
$7t_{1u}^{\uparrow}$	1.026	0.78	13.56	16.28	1.57	S 3*s*
$7t_{1u}^{\downarrow}$	1.029	0.71	13.61	16.09	1.56	S 3*s*
$4e_g^{\uparrow}$	1.014	1.79	13.77	13.62	1.94	S 3*s*
$4e_g^{\downarrow}$	1.015	1.06	13.89	13.60	1.97	S 3*s*
$8a_{1g}^{\uparrow}$	0.433	12.38	8.72	30.78	4.55	S 3*p*, Fe 4*s*
$8a_{1g}^{\downarrow}$	0.421	10.38	9.00	30.93	4.70	S 3*p*, Fe 4*s*
$5e_g^{\uparrow}$	0.474	74.64	2.73	7.19	1.81	Fe 3*d*, S 3*p*
$5e_g^{\downarrow}$	0.333	30.05	7.93	15.81	6.54	S 3*p*, Fe 3*d*
$2t_{2g}^{\uparrow}$	0.465	72.45	2.00	14.61	0.90	Fe 3*d*, S 3*p*
$2t_{2g}^{\downarrow}$	0.384	6.90	8.21	38.28	5.59	S 3*p*, Fe 3*d*
$8t_{1u}^{\uparrow}$	0.373	2.63	8.99	41.16	2.27	S 3*p*
$8t_{1u}^{\downarrow}$	0.372	2.25	9.05	41.18	2.25	S 3*p*
$3t_{2g}^{\uparrow}$	0.333	24.88	6.69	28.73	6.26	S 3*p*, Fe 3*d*
$2t_{2u}^{\uparrow}$	0.289	0.11	10.44	31.23	6.02	S 3*p*
$2t_{2u}^{\downarrow}$	0.289	0.11	10.48	31.07	5.92	S 3*p*
$9t_{1u}^{\uparrow}$	0.269	1.82	10.08	24.74	12.96	S 3*p*
$9t_{1u}^{\downarrow}$	0.269	1.68	10.20	24.32	12.80	S 3*p*
$2t_{1g}^{\uparrow}$	0.249	0.00	10.81	35.14	0.00	S 3*p*
$2t_{1g}^{\downarrow}$	0.252	0.00	10.85	34.90	0.00	S 3*p*
$3t_{2g}^{\downarrow}$[c]	0.144	85.72	0.58	7.92	2.90	Fe 3*d*, S 3*p*
$6e_g^{\uparrow}$	0.177	24.56	8.33	13.89	11.56	S 3*p*, Fe 3*d*

[a]In units of percent of one electron charge.
[b]In units of percent of charge in each S sphere.
[c]Highest occupied level.

μ_B is the Bohr magneton, and S is the total spin. The field H_c may be interpreted in a Hartree-Fock (HF) formalism as originating from the polarization of the s shells by the unpaired d electrons. The other two terms are the orbital and dipolar contributions to the hyperfine field.

From our spin-polarized calculations we obtain charge and spin densities at the nucleus from the a_{1g} orbitals with $l=0$ in the Fe sphere. The Fermi-contact term, which is proportional to the difference in spin-up and spin-down densities at the nucleus could then be calculated. In Tables X–XII we give the total spin density at the Fe nucleus as well as the individual contributions from the different orbitals. For comparison, the same information for the Fe^{2+} (singlet and quintuplet), Fe^{3+} (sextuplet and doublet), and Fe^{4+} (quintuplet and triplet) ions are also included.

Individual contributions to H_c are quite sensitive to covalent effects, i.e., mixing between S $3p$ and Fe $3d$ orbit-

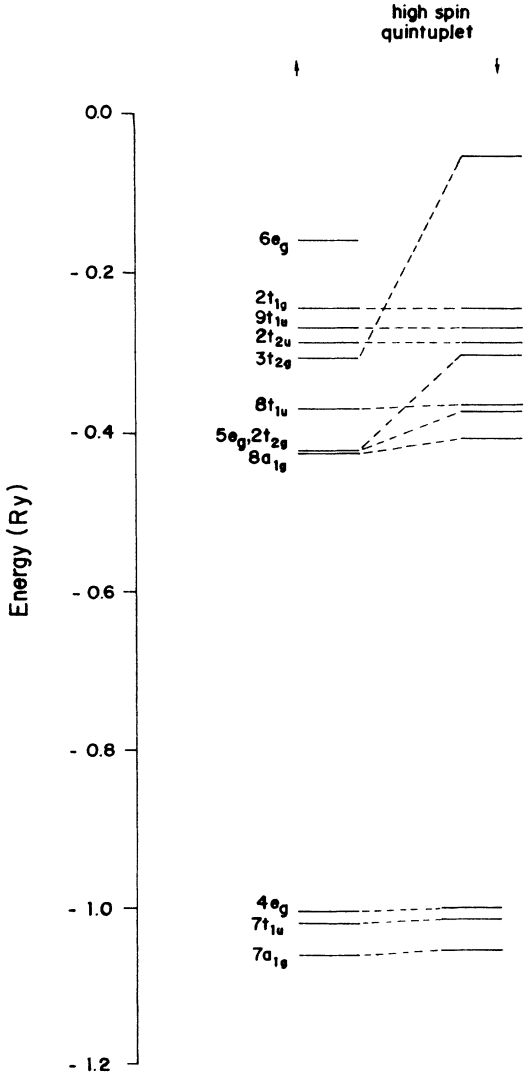

FIG. 1. Orbital energies for the FeS_6^{10-} (quintuplet) cluster.

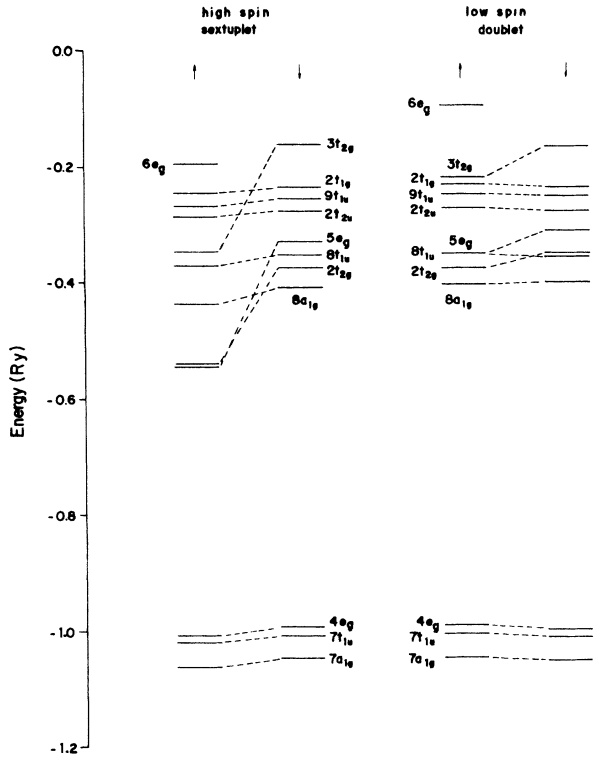

FIG. 2. Orbital energies for the FeS_6^{9-} (doublet and sextuplet) clusters.

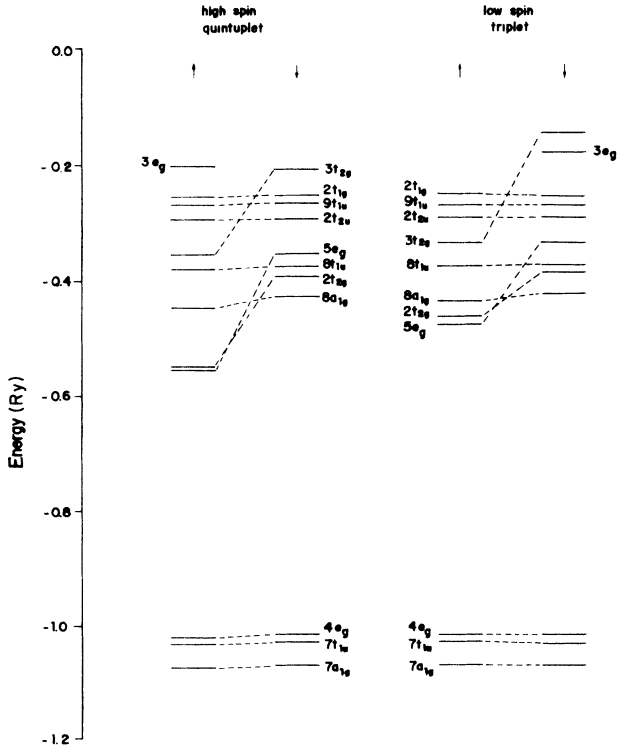

FIG. 3. Orbital energies for the FeS_6^{8-} (triplet and quintuplet) clusters.

TABLE V. Electron population on Fe for molecular orbitals of a_{1g}, e_g, and t_{2g} symmetries for low-spin FeS_6^{10-} ($d_{Fe\text{-}S}=2.26$ Å).

Symmetry	Atomic character	$l=2$ on S	$l=1$ on S
$7a_{1g}$	4s	0.17	0.16
$8a_{1g}$	4s	0.58	0.56
$5e_g$	3d	1.06	0.97
$2t_{2g}$	3d	0.34	0.30
$3t_{2g}$	3d	4.58	4.75
Total charge	3d	5.98	6.02
	4s	0.74	0.72
Net charge on Fe (8 − total)		1.28	1.26

als, partial occupation of the 4s levels, charge delocalization, and exchange polarization effects.

The Fe 3d and 4s populations are $3d_{\uparrow}^{5.00}3d_{\downarrow}^{1.04}4s_{\uparrow}^{0.31}4s_{\downarrow}^{0.29}$ for FeS_6^{10-} (quintuplet) and $3d_{\uparrow}^{4.76}3d_{\downarrow}^{0.82}4s_{\uparrow}^{0.36}4s_{\downarrow}^{0.34}$ for FeS_6^{9-} (sextuplet) clusters, respectively (see Table IX). The main difference between the FeS_6^{9-} (sextuplet) cluster and the Fe^{3+} free ion is an increase of 0.82 electrons in the $3d\downarrow$ level and partial occupation of the 4s shells. For the FeS_6^{10-} (quintuplet) cluster the 3d occupation is the same as for the Fe^{2+} free ion, the only difference being the partial occupation of the 4s shell. From Tables X and XI we find large positive 4s contributions of 205 kG in the FeS_6^{10-} cluster and 243 kG in the FeS_6^{9-} cluster, respectively, which come mainly from the $7a_{1g}$ and $8a_{1g}$ orbitals. We also observe a modification of the 2s and 3s values compared to the free-ion values. For the FeS_6^{9-} cluster the additional partial population of the $3d_{\downarrow}$ orbitals will reduce the magnitude of the negative and positive 2s and 3s spin contributions, respectively. (See Table XII for aspects of the FeS_6^{8-} cluster.)

In the FeS_6^{10-} cluster there is no significant change of the $3d_{\downarrow}$ population and there is also not a significant change of the 2s and 3s spin contributions with respect to Fe^{2+} (quintuplet) free-ion values as compared to the FeS_6^{9-} cluster.

The calculated hyperfine field in the FeS_6^{10-} (quintuplet) cluster (Table X) is −311 kG, and −296 kG in the FeS_6^{9-} cluster (Table XI). Coey *et al.*[32] found a hyperfine field of 310 kG at *B* sites, in good agreement with our theoretical value. They had also suggested electron hopping between ferrous and ferric sites. We note that if both high-spin Fe(II) and Fe(III) sites have similar values of magnetic hyperfine fields, as suggested by our present calculations, there may be difficulties in distinguishing unambiguously the Fe^{2+} and Fe^{3+} octahedral sites expected for an inverse spinel. We note, however, that we have neglected possible orbital and dipolar contributions.

Our calculations in Table XI indicate that there should only be a small contribution of 56 kG from the Fermi-contact term to the magnetic hyperfine interaction in the FeS_6^{9-} (doublet) configuration. Thus in the few cases where the low-spin Fe(III) configuration may occur, if there are not significant orbital or dipolar contributions, then the magnetic hyperfine splitting may be difficult to detect. Mössbauer-effect studies of several intermediate-spin Fe(III) compounds indicate that most of these compounds are simple paramagnets.[35]

The Mössbauer isomer shift (IS) is defined as

$$\delta=\tfrac{2}{3}\pi Ze^2S(Z)\Delta\langle r^2\rangle[\rho_A(0)-\rho_S(0)]=\alpha\,\Delta\rho(0)\ , \qquad (3)$$

where $\Delta\langle r^2\rangle$ is the change in the mean-square nuclear charge radius in the Mössbauer transition (negative for Fe) and the term in square brackets is the difference between the squared amplitude of the electronic wave function at the nucleus of absorber and source. $S(Z)$ is a

TABLE VI. Electron population on Fe for molecular orbitals of a_{1g}, e_g, and t_{2g} symmetries for high-spin FeS_6^{10-} ($d_{Fe\text{-}S}=2.46$ Å).

Symmetry	Atomic character	$l=2$ on S		$l=1$ on S	
$7a_{1g}$	4s	0.04	0.04	0.04	0.04
$8a_{1g}$	4s	0.27	0.25	0.27	0.25
$5e_g$	3d	1.25	0.28	1.22	0.27
$6e_g$	3d	0.80	0.00	0.83	0.00
$2t_{2g}$	3d	1.31	0.07	1.31	0.07
$3t_{2g}$	3d	1.64	0.71	1.64	0.70
Total charge	3d	5.00	1.06	5.00	1.04
	4s	0.31	0.29	0.31	0.29
Net charge on Fe (8 − total)		1.34		1.36	

TABLE VII. Electron population on Fe for molecular orbitals of a_{1g}, e_g, and t_{2g} symmetries for FeS_6^{9-}.

Symmetry	Atomic character	High spin		Low spin	
$7a_{1g}$	4s	0.05	0.05	0.04	0.04
$8a_{1g}$	4s	0.31	0.29	0.25	0.26
$5e_g$	3d	1.70	0.60	0.84	0.22
$2t_{2g}$	3d	2.71	0.22	0.42	0.13
$3t_{2g}$	3d	0.35	0.00	2.47	1.77
Total	3d	4.76	0.82	3.73	2.12
charge	4s	0.36	0.34	0.29	0.30
Net charge on Fe (8−total)		1.72		1.56	

correction term for relativistic effects and α is the IS calibration constant which contains all nuclear parameters.

The Mössbauer IS's in Fe octahedral sulfides are larger than those observed for the Fe tetrahedral sulfides since the metal-ligand distances are shorter for tetrahedral coordination and both covalency and core distorsions are correspondingly larger. Ligand-Fe interaction via 4s contribution and delocalization of 3d electrons should increase the charge density at the nucleus, thereby reducing the IS from the free-ion value. However, covalency involving charge transfer from the ligand to the 3d orbitals should have an opposite effect. The increase in the radial extension of the 3d orbital by covalency should also be considered.

In Tables XIII–XV we give the total charge densities and individual contributions for the FeS_6^{10-} (singlet and quintuplet, with $l=1$ and 2 on the S sphere), FeS_6^{9-} (sextuplet and doublet), and FeS_6^{8-} (quintuplet and triplet) clusters. The values for the high- and low-spin Fe^{2+}, Fe^{3+}, and Fe^{4+} configurations are also given for comparison. In the FeS_6^{9-} (sextuplet and doublet) and FeS_6^{8-} (quintuplet and triplet) clusters, we observe a decrease of the 3s contributions relative to free-ion values due to increased shielding of the nuclear charge caused by the increased 3d population in these clusters. In the FeS_6^{10-} (singlet and quintuplet) clusters we do not find significant modification of the 3d population and thus also no significant change of the 3s contribution to the total charge density at the Fe nucleus. Then, from calculated charge densities (ρ_i,ρ_j) and measured IS's, the IS calibration constant α is determined by

$$\delta_i-\delta_j=\alpha[\rho_i(0)-\rho_j(0)]\ , \tag{4}$$

where the lower index refers to different chemical compounds.

Vaughan and Ridout[33] gives the experimental IS in greigite at Fe^{2+} octahedral B sites as ± 0.70 mm/s and that at Fe^{3+} octahedral B sites as $+0.45$ mm/s. Using these experimental values and the electron densities for the FeS_6^{10-} and FeS_6^{9-} high-spin clusters, we obtain an IS calibration constant of $\alpha=-0.27a_0^3$ mm/s, which is

TABLE VIII. Electron population on Fe for molecular orbitals of a_{1g}, e_g, and t_{2g} symmetries for FeS_6^{8-}.

Symmetry	Atomic character	High spin		Low spin	
$7a_{1g}$	4s	0.05	0.05	0.05	0.05
$8a_{1g}$	4s	0.32	0.30	0.29	0.28
$5e_g$	3d	1.70	0.72	1.47	0.49
$6e_g$	3d	0.21	0.00	0.00	0.00
$2t_{2g}$	3d	2.73	0.30	2.17	0.16
$3t_{2g}$	3d	0.00	0.00	0.85	0.88
Total	3d	4.64	1.02	4.49	1.53
charge	4s	0.37	0.35	0.34	0.33
Net charge on Fe (8−total)		1.62		1.31	

TABLE IX. Net charge and $3d$ and $4s$ populations for FeS_6^{10-}, FeS_6^{9-}, and FeS_6^{8-} clusters.

	Net Fe charge	$3d$-electron population	$4s$-electron population
FeS_6^{-8} [a]	1.62	$3d_{\uparrow}^{4.64}3d_{\downarrow}^{1.02}$	$4s_{\uparrow}^{0.37}4s_{\downarrow}^{0.35}$
FeS_6^{-8} [b]	1.31	$3d_{\uparrow}^{4.49}3d_{\downarrow}^{1.53}$	$4s_{\uparrow}^{0.34}4s_{\downarrow}^{0.33}$
FeS_6^{-9} [a]	1.72	$3d_{\uparrow}^{4.76}3d_{\downarrow}^{0.82}$	$4s_{\uparrow}^{0.36}4s_{\downarrow}^{0.34}$
FeS_6^{-9} [b]	1.56	$3d_{\uparrow}^{3.73}3d_{\downarrow}^{2.12}$	$4s_{\uparrow}^{0.29}4s_{\downarrow}^{0.30}$
FeS_6^{-10} [c]	1.26	$3d^{6.02}$	$4s^{0.72}$
FeS_6^{-10} [d]	1.28	$3d^{5.98}$	$4s^{0.74}$
FeS_6^{-10} [e]	1.36	$3d_{\uparrow}^{5.00}3d_{\downarrow}^{1.04}$	$4s_{\uparrow}^{0.31}4s_{\downarrow}^{0.29}$
FeS_6^{-10} [f]	1.34	$3d_{\uparrow}^{5.00}3d_{\downarrow}^{1.06}$	$4s_{\uparrow}^{0.31}4s_{\downarrow}^{0.29}$

[a]High spin.
[b]Low spin.
[c]Low-spin l up to 1 on S.
[d]Low-spin l up to 2 on S.
[e]High-spin l up to 1 on S.
[f]High-spin l up to 2 on S.

slightly larger than the currently assumed value of $-0.22a_0^3$ mm/s. As emphasized by Goodenough and Fatseas[37] and Coey *et al.*,[32] it may be necessary to consider fast relaxation rates, mean values of valence, and IS's in tetrahedral and octahedral iron sulfides in order to interpret the measured IS in greigite.

Since iron pyrite contains low-spin Fe^{2+}, there should be no contribution from this S state to the electric field gradient. The observed electric field gradient must arise from some other mechanism. Possible causes include low site symmetry for the Fe atoms or an anisotropic mean-square displacement of the Fe atoms. It has been shown, however, that neither crystal-field effects nor non-stoichiometry are enough to account for the observed splitting. A very small amount of electron delocalization, however, may be enough to cause the observed splitting because of the strong effect the valence electrons have on the Fe nucleus.

The observed quadrupole splitting due to low-spin Fe^{2+} in FeS_2 (pyrite) is 0.64 mm/s. The valence-shell contribution to the Mössbauer quadrupole splitting (QS) can be expressed as

$$\Delta_{QS}=\tfrac{1}{2}e^2q_{val}(1-R)Q\ , \tag{5}$$

$$q_{val}=\sum\langle 3\cos^2\theta-1\rangle\langle r^{-3}\rangle\ . \tag{6}$$

Here, R is the Sternheimer antishielding factor, and Q is the nuclear quadrupole moment. From symmetry properties of the wave function, the d-electron contribution to q_{val} can be expressed as

$$q_{val}=K_d[-N_{d_{z^2}}+N_{d_{x^2-y^2}}+N_{d_{xy}}-\tfrac{1}{2}(N_{d_{xz}}+N_{d_{yz}})]\ , \tag{7}$$

$$K_d=\tfrac{4}{7}\langle r^{-3}\rangle_d\ . \tag{8}$$

We note from Eq. (7) that if the e_g and t_{2g} orbitals are

TABLE X. Spin densities χ $[\chi=4\pi\sum_i|\,|u_{\uparrow}^i(0)|^2-|u_{\downarrow}^i(0)|^2\,|$, where u^i is an occupied orbital of a_1 symmetry or an atomic s orbital] at the Fe nucleus and Fermi-contact term H_c for the high-spin FeS_6^{10-} cluster and Fe^{2+} free ion.

	$l=2$ on S	$l=1$ on S		Fe^{2+}
$1a_{1g}$ (Fe $1s$)	−0.76	−0.89	$1s$	−0.81
$3a_{1g}$ (Fe $2s$)	−22.04	−22.67	$2s$	−23.31
$6a_{1g}$ (Fe $3s$)	11.02	11.31	$3s$	+10.41
$7a_{1g}$	0.55	0.57		
$8a_{1g}$	4.27	4.29		
Total	−6.96	−7.39	Total	−13.71
H_c (kG)	−293	−311	H_c (kG)	−577

TABLE XI. Spin densities χ $[\chi=4\pi\sum_i|\,|u_{\uparrow}^i(0)|^2-|u_{\downarrow}^i(0)|^2\,|$, where u^i is an occupied orbital of a_1 symmetry or an atomic s orbital] at the Fe nucleus and Fermi-contact term H_c for the FeS_6^{9-} cluster and Fe^{3+} free ion.

High-spin FeS_6^{9-}		Fe^{3+}	
$1a_{1g}$ (Fe $1s$)	−0.89	$1s$	−1.14
$3a_{1g}$ (Fe $2s$)	−24.54	$2s$	−32.63
$6a_{1g}$ (Fe $3s$)	12.63	$3s$	15.17
$7a_{1g}$	0.67		
$8a_{1g}$	5.10		
Total	−7.03	Total	−18.60
H_c (kG)	−296	H_c (kG)	−783
Low-spin FeS_6^{9-}		**Fe^{3+}**	
$1a_{1g}$ (Fe $1s$)	−0.38	$1s$	−0.00
$3a_{1g}$ (Fe $2s$)	−8.48	$2s$	−6.56
$6a_{1g}$ (Fe $3s$)	4.19	$3s$	+3.24
$7a_{1g}$	0.48		
$8a_{1g}$	2.87		
Total	−1.32	Total	−3.32
H_c (kG)	−56	H_c (kG)	−139

TABLE XII. Spin densities χ [$\chi=4\pi\sum_i |\,|u'_\uparrow(0)|^2 - |u'_\downarrow(0)|^2\,|$, where u' is an occupied orbital of a_1 symmetry or an atomic s orbital] at the Fe nucleus and Fermi-contact term H_c for the FeS_6^{8-} cluster and Fe^{4+} free ion.

High-spin FeS_6^{8-}		Fe^{4+}	
$1a_{1g}$ (Fe 1s)	−0.76	1s	−1.04
$3a_{1g}$ (Fe 2s)	−22.41	2s	−29.13
$6a_{1g}$ (Fe 3s)	11.54	3s	14.76
$7a_{1g}$	0.67		
$8a_{1g}$	5.00		
Total	−5.96	Total	−15.41
H_c (kG)	−251	H_c (kG)	−648
Low-spin FeS_6^{8-}		Fe^{4+}	
$1a_{1g}$ (Fe 1s)	−0.63	1s	−0.25
$3a_{1g}$ (Fe 2s)	−19.81	2s	−14.54
$6a_{1g}$ (Fe 3s)	10.24	3s	7.57
$7a_{1g}$	0.57		
$8a_{1g}$	4.22		
Total	−5.41	Total	−7.22
H_c (kG)	−228	H_c (kG)	−304

equally populated, $q_{val}=0$. If, however, there is some delocalization or charge transfer to the metal, a nonzero q_{val} can result and produce a quadrupole splitting. Finklea *et al.*[43] have noted that, in pyrite,

$$-N_{d_{z^2}}+N_{d_{x^2-y^2}}+N_{d_{xy}}-\tfrac{1}{2}(N_{d_{xz}}+N_{d_{yz}})=-0.0336 \quad (9)$$

is the necessary 3d population change required to produce a QS of 0.64 mm/s. We note from Table V that the difference between the average total e_g and t_{2g} spin-up and spin-down 3d populations is 0.04, in good agreement with the value predicted from experiment. This agreement may be fortuitous, however, considering the approximations involved. The important conclusion is that our calculated 3d population can account for the order of magnitude of the observed quadrupole splitting.

TABLE XIII. Electron densities $|\psi(0)|^2$ [$|\psi(0)|^2 = \sum_i |\psi'_\uparrow(0)|^2 + |\psi'_\downarrow(0)|^2$] at the Fe nucleus for low- and high-spin FeS_6^{10-} clusters and Fe^{2+} free ion.

	$l=2$ on S	$l=1$ on S		Fe^{2+}
		Low spin		
$1a_{1g}$ (Fe 1s)	10 754.36	10 754.36	1s	10 752.49
$3a_{1g}$ (Fe 2s)	980.45	980.41	2s	978.98
$6a_{1g}$ (Fe 3s)	141.93	141.79	3s	141.96
$7a_{1g}$	0.93	0.91		
$8a_{1g}$	3.30	3.10		
Total	11 880.97	11 880.57		11 873.16
		High spin		
$1a_{1g}$ (Fe 1s)	10 754.44	10 754.49	1s	10 752.46
$3a_{1g}$ (Fe 2s)	980.44	980.44	2s	979.06
$6a_{1g}$ (Fe 3s)	141.87	141.77	3s	141.41
$7a_{1g}$	0.50	0.50		
$8a_{1g}$	3.04	2.96		
Total	11 880.29	11 880.16		11 872.93

TABLE XIV. Electron densities $|\psi(0)|^2$ [$|\psi(0)|^2 = \sum_i |\psi'_\uparrow(0)|^2 + |\psi'_\downarrow(0)|^2$] at the Fe nucleus for the FeS_6^{9-} cluster and Fe^{3+} free ion.

High-spin FeS_6^{9-}		Fe^{3+}	
$1a_{1g}$ (Fe 1s)	10 754.43	1s	10 751.84
$3a_{1g}$ (Fe 2s)	980.41	2s	978.98
$6a_{1g}$ (Fe 3s)	142.22	3s	143.85
$7a_{1g}$	0.57		
$8a_{1g}$	3.45		
Total	11 881.08		11 874.67
Low-spin FeS_6^{9-}		Fe^{3+}	
$1a_{1g}$ (Fe 1s)	10 754.50	1s	10 752.19
$3a_{1g}$ (Fe 2s)	980.43	2s	978.88
$6a_{1g}$ (Fe 3s)	142.12	3s	144.28
$7a_{1g}$	0.48		
$8a_{1g}$	2.87		
Total	11 880.40		11 875.35

The measured magnetic moment[31] of $(2.2\pm0.3)\mu_B$/molecule in greigite is inconsistent with all assignments of high- or low-spin (Fe^{2+},Fe^{3+}) cations to the A and B sites. Using spin-only values for the ionic moments, one obtains a net moment $\geq 4\mu_B$. Furthermore, the conductivity shows that there must be delocalized charge in the compound. Goodenough[37] has taken account of covalency effects in sulfides by proposing that the $t_2(A)$ and $e_g(B)$ electrons are delocalized into a σ^* band which is unpolarized. As long as σ^* is to remain unpolarized, $t_{2g}(B)$ spin down may accept electrons in pairs and effectively reduce the net magnetic moment.

TABLE XV. Electron densities $|\psi(0)|^2$ [$|\psi(0)|^2 = \sum_i |\psi'_\uparrow(0)|^2 + |\psi'_\downarrow(0)|^2$] at the Fe nucleus for the FeS_6^{8-} cluster and Fe^{4+} free ion.

High-spin FeS_6^{8-}		Fe^{4+}	
$1a_{1g}$ (Fe 1s)	10 754.42	1s	10 751.76
$3a_{1g}$ (Fe 2s)	982.19	2s	978.99
$6a_{1g}$ (Fe 3s)	142.31	3s	147.73
$7a_{1g}$	0.59		
$8a_{1g}$	3.51		
Total	11 883.02		11 878.48
Low-spin FeS_6^{8-}		Fe^{4+}	
$1a_{1g}$ (Fe 1s)	10 754.41	1s	10 751.74
$3a_{1g}$ (Fe 2s)	980.39	2s	978.91
$6a_{1g}$ (Fe 3s)	142.01	3s	147.97
$7a_{1g}$	0.53		
$8a_{1g}$	3.26		
Total	11 880.60		11 878.62

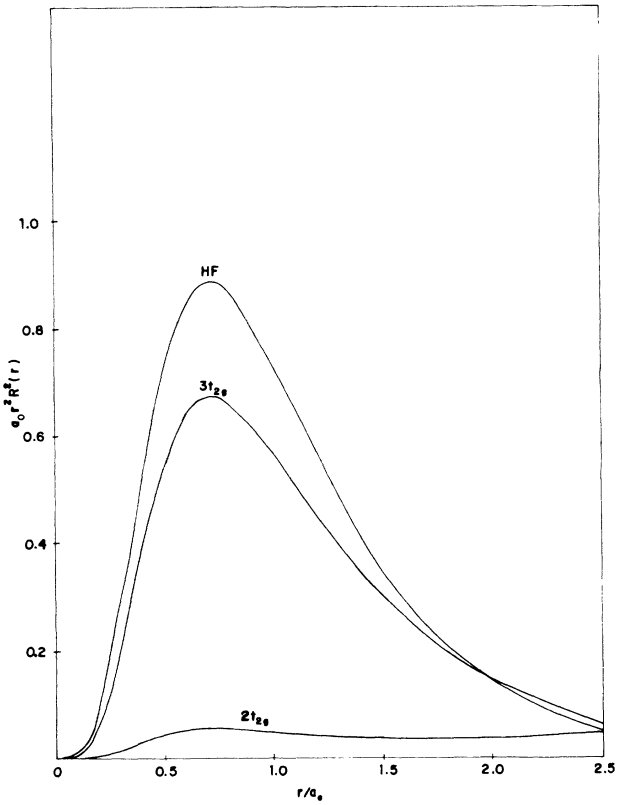

FIG. 4. Radial densities of t_{2g} orbitals of FeS_6^{10-} (singlet) cluster. Fe^{2+} (singlet) HF $X\alpha$ density given for comparison.

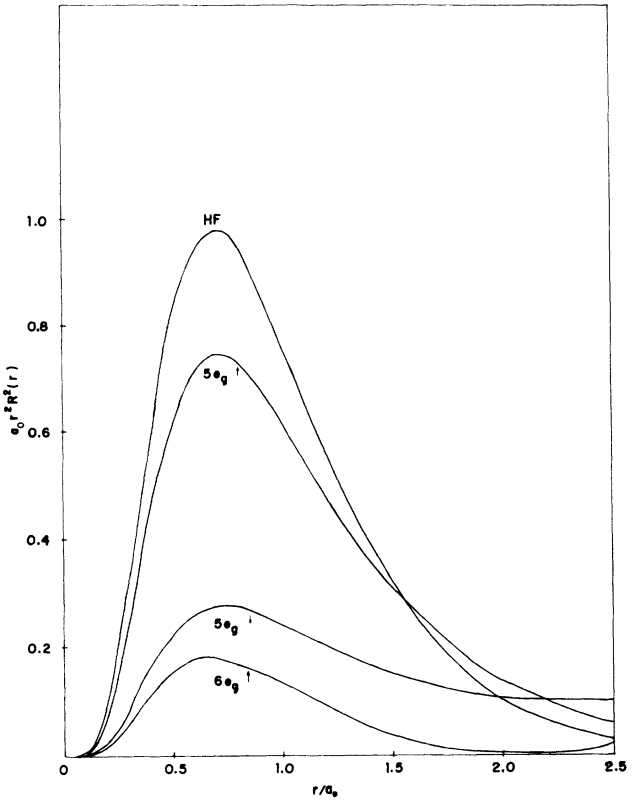

FIG. 6. Radial densities of e_g orbitals of FeS_6^{9-} (sextuplet). Fe^{3+} (sextuplet) HF $X\alpha$ density given for comparison.

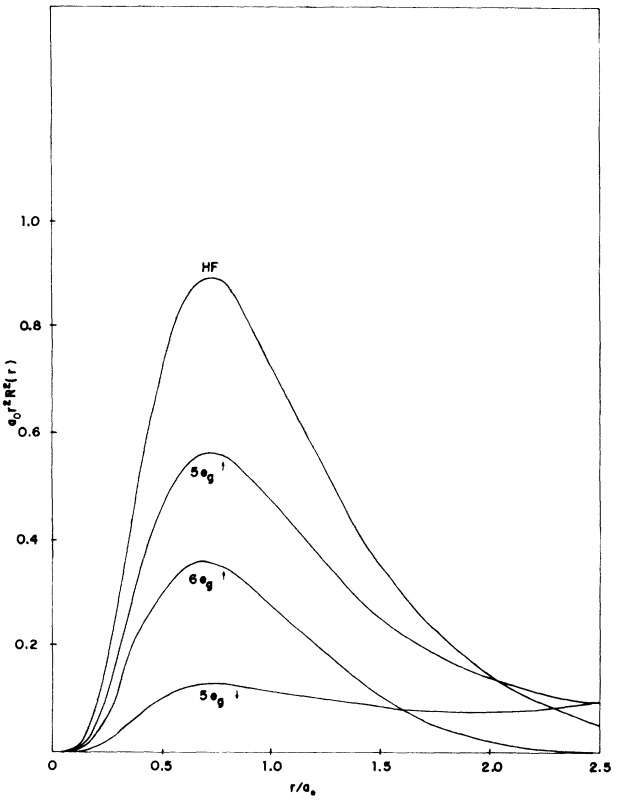

FIG. 5. Radial densities of e_g orbitals of FeS_6^{10-} (quintuplet) cluster. Fe^{2+} (quintuplet) HF $X\alpha$ density given for comparison.

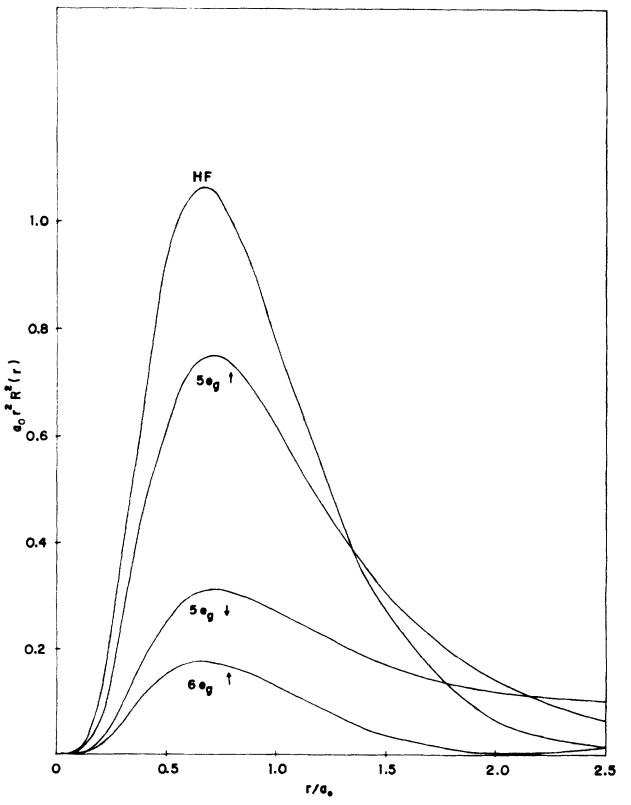

FIG. 7. Radial densities of e_g orbitals FeS_6^{8-} (quintuplet). Fe^{4+} (quintuplet) HF $X\alpha$ density given for comparison.

TABLE XVI. Fe 3*s* and 4*s* contributions to the electron density $|\psi(0)|^2$ for the selected clusters and spin configurations.

Cluster	3*s* contribution	4*s* contribution
FeS_6^{10-} ($l=2$ on S, singlet)	141.93	4.23
FeS_6^{10-} ($l=1$ on S, singlet)	141.79	4.01
FeS_6^{10-} ($l=2$ on S, quintet)	141.87	3.54
FeS_6^{10-} ($l=1$ on S, quintet)	141.77	3.46
FeS_6^{9-} (sextuplet)	142.22	4.02
FeS_6^{9-} (duplet)	142.12	3.35
FeS_6^{8-} (quintet)	142.31	4.10
FeS_6^{8-} (triplet)	142.01	3.79
Free atom		
$3d^6 4s^2$	141.71	8.92
$3d^6$	141.41	
$3d^5 4s^2$	143.63	13.22
$3d^5$	143.85	
$3d^4 4s^2$	147.00	18.05
$3d^4$	147.73	

We thus assume that the localized 3*d* electrons responsible for the net magnetic moment are the e (Fe^{3+}) electrons at A tetrahedral sites as well as the t_{2g} (Fe^{2+},Fe^{3+}) electrons at B octahedral sites. From Tables VI and VII we set that there are 2.18 unpaired $t_{2g}(3d)$ electrons for octahedral Fe^{2+} and 2.84 electrons for high-spin Fe^{3+}. The net magnetic moment per molecule is $\approx(2.84+2.18-2.0)\mu_B=3.02\mu_B$.

A second band scheme by Spender *et al.*[31] is based on the idea that greigite has only ferrous ions on B sites. In this case the net magnetic moment would be $(2\times2.18-2.0)\mu_B=2.36\mu_B$, in agreement with the experimental value of $(2.2\pm0.3)\mu_B$. Although it is not possible to draw firm conclusions from these estimates, they nevertheless suggest that there may be some fast electronic relaxation at the B site between the two species upon reduction of one ferric ion by sulfur to the ferrous state as suggested by Coey *et al.*[32] and by Spender *et al.*[31] Goodenough[37] comments that it is of particular interest whether the reduction of the atomic moments in greigite is due to charge transfer from the S^{2-} $3p^6$ valence band to the octahedral site Fe $3d^6$ bands or to a delocalization of the Fe 3*d* electrons that form σ bonds to S.

Our calculations indicate that in both the Fe^{2+} and Fe^{3+} high-spin configurations expected in greigite, there is a partial population of the Fe 3*d* spin-down orbitals, whereas Fe 3*d* delocalization seems to mostly occur in the Fe^{3+} high-spin configuration.

In Figs. 4–7 we plot the most interesting radial densities for the FeS_6^{10-} (singlet and quintuplet) as well as the FeS_6^{9-} (sextuplet) and FeS_6^{8-} (quintuplet) clusters. The HF $X\alpha$ Fe^{2+}, Fe^{3+}, and Fe^{4+} free-ion radial densities are also given for comparison. The Fe 3*d* and 4*s* orbitals are quite sensitive to bonding, tending to delocalize and mix charge from the ligand 3*p* orbitals with the Fe 3*d* and 4*s* levels with significant effects on electric magnetic and hyperfine parameters. In the Fe sphere both the $3d_\uparrow$ and $3d_\downarrow$ e_g and t_{2g} occupied and unoccupied radial functions have nearly atomiclike 3*d* shape, with maxima in the same region as the corresponding free ions (Fe^{2+}, Fe^{3+}, and Fe^{4+}). We note (Fig. 4) that the t_{2g} 3*d* charge densities are contained within the free-ion charge density, whereas there is some delocalization of the higher e_g levels (Figs. 5–7) on the S sphere. Thus, although our cluster model cannot give the information obtained from band models, there is nevertheless tendency for the t_{2g} 3*d* orbitals to be more localized than the energetically higher e_g 3*d* orbitals. (See Table XVI.)

The present MS $X\alpha$ calculations therefore describe the main features of the bonding in octahedral FeS_6^{n-} ($n=8,9,10$) clusters which significantly affect the measured Mössbauer hyperfine parameters, magnetic moments, and the stability of these compounds for different valence and spin configurations.

ACKNOWLEDGMENTS

One of us (M.B.) acknowledges financial support from Conselho Nacional de Desenvolvimento Científico e Tecnológico (CNPq). C.A.T. and W.A.L. acknowledge support from the U.S. National Science Foundation–CNPq (Brazil) International Exchange Research Collaboration Program. W.A.L. was supported in part by the Director, Office of Energy Research, Office of Basic Energy Sciences, Chemical Sciences Division of the U.S. Department of Energy under Contract No. DE-AC03-76SF00048.

[1]C. A. Taft, D. Raj, and J. Danon, in Proceedings of the International Conference on Mössbauer Spectroscopy, Bendor, France, 1974 [J. Phys. (Paris) Colloq. **35**, C6-241 (1974)].

[2]C. A. Taft, S. F. Cunha, N. G. Souza, and N. C. Furtado, J. Phys. Chem. Solids **41**, 61 (1980).

[3]C. A. Taft, J. Phys. (Paris) **38**, 15 (1977).

[4]R. B. Scorzelli, C. A. Taft, J. Danon, and V. K. Garg, J. Phys. C **11**, 1397 (1978).

[5]R. S. de Biasi, C. A. Taft, and N. C. Furtado, J. Magn. Magn. Mater. **23**, 211 (1981).

[6]T. P. Arsenio, Z. Arguello, P. H. Domingues, N. C. Furtado, and C. A. Taft, Phys. Status Solidi **110**, K129 (1982).

[7]C. A. Taft and M. A. de Paoli, Chem. Phys. Lett. **68**, 94 (1979).

[8]P. H. Domingues, T. P. Arsenio, N. C. Furtado, and C. A. Taft, Phys. Status Solidi B **114**, K161 (1982).

[9]D. M. Cooper, D. P. E. Dickson, P. H. Domingues, G. P. Gupta, C. E. Johnson, M. F. Thomas, C. A. Taft, and P. J. Walker, J. Magn. Magn. Mater. **36**, 171 (1983).

[10]R. S. de Biasi, C. A. Taft, and N. C. Furtado, J. Magn. Magn. Mater. **21**, 125 (1980).

[11]T. P. Arsenio, P. H. Domingues, and C. A. Taft, Phys. Status Solidi B **105**, K31 (1981).

[12]D. J. Vaughan and J. R. Craig, *Mineral Chemistry of Metal Sulfides* (Cambridge University Press, New York, 1978).

[13]P. H. Domingues, J. M. Neto, C. A. Taft, N. C. Furtado, and T. P. Arsenio, Solid State Commun. **56**, 193 (1985).

[14]R. S. de Biasi, C. A. Taft, and N. C. Furtado, J. Mater. Sci. Lett. **5**, 1191 (1986).
[15]I. L. Torriani, Z. P. Arguello, A. R. Freiria Filho, J. P. Suassuna, and C. A. Taft, J. Mater. Sci. **23**, 1068 (1988).
[16]R. S. de Biasi, C. A. Taft, and N. C. Furtado, J. Mater. Sci. Lett. **6**, 1185 (1987).
[17]Y. K. Sharma, L. Iannarella, F. E. Wagner, C. A. Taft, N. C. Furtado, and T. P. Arsenio, in Proceedings of the International Conference on Applications of Mössbauer Spectroscopy, Canberra, 1987 [Hyperfine Interact. **41**, 517 (1988)].
[18]J. T. Hoggins and H. Steinfink, Inorg. Chem. **15**, 1682 (1976).
[19]M. Eibschutz, S. Shtrikman, and Y. Tenenbaum, Phys. Lett. **24A**, 563 (1967); M. R. Spender and A. H. Morrish, Can. J. Phys. **50**, 1125 (1972).
[20]C. Garcin, P. Imbert, G. Jéhanno, A. Gérard, and J. Danon, J. Phys. Chem. Solids **41**, 969 (1980).
[21]C. A. Taft and M. Braga, Phys. Rev. B **21**, 5802 (1980).
[22]S. K. Lie and C. A. Taft, Chem. Phys. Lett. **89**, 463 (1982).
[23]S. K. Lie and C. A. Taft, Phys. Rev. B **28**, 7308 (1983).
[24]S. K. Lie, M. Braga, and C. A. Taft, Phys. Rev. B **38**, 4382 (1988).
[25]N. C. Furtado, C. A. Taft, and J. O. Cassedane, J. Mater. Sci. (to be published).
[26]J. A. Tossell, J. Chem. Phys. **66**, 5712 (1977).
[27]S. Lauer, A. X. Trautwein, and F. E. Harris, Phys. Rev. B **29**, 6774 (1984).
[28]R. G. Burns and D. J. Vaughan, Am. Mineral. **55**, 1576 (1970).
[29]A. Kjekshus and D. G. Nicholson, Acta Chem. Scand. **25**, 866 (1971).
[30]J. A. Morice, L. V. C. Rees, and D. T. Rickard, J. Inorg. Nucl. Chem. **31**, 3797 (1969).
[31]M. R. Spender, J. M. D. Coey, and A. H. Morrish, Can. J. Phys. **50**, 2313 (1972).
[32]J. M. D. Coey, M. R. Spender, and A. H. Morrish, Solid State Commun. **18**, 1605 (1970).
[33]D. J. Vaughan and M. S. Ridout, J. Inorg. Nucl. Chem. **33**, 741 (1971).
[34]E. K. Li, K. H. Johnson, D. E. Eastman, and J. L. Freeout, Phys. Rev. Lett. **32**, 470 (1974).
[35]H. H. Wickman and A. M. Tronzzolo, Inorg. Chem. **7**, 63 (1968).
[36]D. Niarchos and D. Cebrides, Chem. Phys. **41**, 97 (1979).
[37]J. B. Goodenough and G. A. Fatseas, J. Solid State Chem. **41**, 1 (1982).
[38]K. H. Johnson, J. Chem. Phys. **45**, 3085 (1966); Adv. Quantum Chem. **7**, 143 (1973).
[39]K. Schwarz, Phys. Rev. B **5**, 2466 (1972).
[40]L. Pauling, *The Nature of the Chemical Bond,* 3rd ed. (Cornell University Press, Ithaca, 1960).
[41]S. Larsson, Theor. Chem. Acta **49**, 45 (1978).
[42]S. Larsson and M. Braga, Int. J. Quantum Chem. **15**, 1 (1979); M. Braga, S. Larsson, and J. R. Leite, J. Am. Chem. Soc. **101**, 3867 (1979); M. Braga, A. C. Pavão, and J. R. Leite, Phys. Rev. B **23**, 4328 (1981).
[43]S. L. Finklea III, LeConte Calhey, and E. L. Alma, Acta Crystallogr. Sect. A **32**, 529 (1976).